Particle precipitation by bipolar corona discharge ion winds

Van Thanh Dau[1], Thien Xuan Dinh[2], Canh-Dung Tran[3], Tibor Terebessy[4], Trinh Chu Duc[5] and Tung Thanh Bui[5]

[1] *Research Group (Environmental Health), Sumitomo Chemical. Ltd, Hyogo 665-8555, Japan (dauv@sc.sumitomo-chem.co.jp; dauthanhvan@gmail.com)*
[2] *Graduate School of Science and Engineering, Ritsumeikan University, Shiga 525-8577, Japan (thien@cfd.ritsumei.ac.jp)*
[3]*School of Mechanical and Electrical Engineering, University of Southern Queensland, Australia (Canh-Dung.Tran@usq.edu.au)*
[4] *Atrium Innovation Ltd., Lupton Road, OX10 9BT, Wallingford, United Kingdom (tibor.terebessy@clearview-intelligence.com)*
[5] *University of Engineering and Technology, Vietnam National University, Hanoi, Vietnam (tungbt@vnu.edu.vn)*

Abstract: The paper reports the development of a particle precipitation based aerosol sampler using bipolar corona discharge ion winds with collected particles of minimized net charge. For the new approach, neutralized particles move towards a sampler under the effect of electric field and dual ion winds. Since there is no electrode or sampling chip installed inside the air-flow channel, impediments to airborne particle flow or ion winds are removed along the flow direction. In addition, the isolation of ion winds, which generate circuit, allows using various materials for the sampling chip including non-conductors and also protecting collected particles from any discharge ignition on the chip. The device mechanism is numerically simulated in OpenFOAM to study the electrofluidodynamic interaction of charged particles and bipolar ion winds. The efficiency of the new approach has been investigated by experiment with a maximum efficiency of 94%. The effects of flow rate, discharge voltage and electrode distances on the method are also evaluated.

Keywords: Charged particles, ionic wind, particle simulation, corona discharge, OpenFOAM

1. Introduction

Research in the healthcare shows that the particulate matter (PM) causes up to 30% of the total burden of diseases [1]. The inhalation of PM could yield numerous lung diseases such as pulmonary fibrosis [2], pulmonary inflammation, pleural effusion, granuloma [3] and cancer risk [4]. Thus, the particle sampling in bio-technology has attracted significant effort to develop new techniques in various application areas, especially in the biomedical engineering. The main objective of the sampling is to collect a sample of airborne particles and then transport them to a detection unit. The active sampling devices are designed based on three major collection methods: the impaction, impingement and filtration [5]. For the impaction approach, the sampling is carried out by the collision of particles to a wall and called as the inertial impaction. Meanwhile in the impingement scheme, a flow of particles is channelled to a collection chamber through nozzles of an air jet. The number of collected particles depends on the air jet characteristics such as the nozzle geometry and the particles' diameter [6–8]. Several commercial devices using this technique include Coriolis® μ air sampler [9] and Bio-sampler [10]. For the filtration method, particles are collected by driving air through a membrane of high density [11–14]. Similar to the impaction technique, devices using the filtration scheme would be overloaded when working in highly contaminated environments [15]. Among sampling devices, the electrostatic precipitator (EP) is evaluated as an efficient technique to filter nanoparticles at low pressure drop [16–19]. This technique is usually applied in bioengineering because it provides softer collection for sensitive micro-organisms which request a slow landing velocity on a substrate [20]. For this approach, a flow of particles is ionized at the upstream by an ionizer [21] before going through an electric field created by a pair of electrodes placed at the downstream of channel as described in Mainelis [22]. Most commonly, an electrostatic precipitator is developed for airborne nanoparticles

using a needle tip to generate a strong field towards a ground plate [23]. Another automated electrostatic sampler for bio-aerosol was proposed [24] using a sphere ground electrode installed at the entrance of aerosol and a sampling high voltage electrode placed in the middle of air channel. Several modifications of this approach were carried out as follows. Instead of sphere ground electrode, a pair of pins is placed in parallel with the aerosol direction and surrounded by a sheath flow while the sampling electrode is installed in the middle of the flow direction and connected to ground [21]. Lee et al. utilized the point-to-plane configuration to create an electric field across the aerosol direction drifting the aerosol to a plane of liquid [25]. Park and his co-workers [26] also used the same configuration but with a liquid covered counter electrode drained out to an adenosine triphosphate bioluminescence array in order to detect the increase of bioluminescent shortly. Another type of electrostatic generated in axisymmetric configuration is wire-to-cylinder with a high voltage electrode applied on the outer wall and the inner wall acts as the sampling stag [27–29]. In spite of many significant progresses, there are several concerns for the mentioned techniques using the conventional corona discharge with single polarity (uni-polarity). Indeed, although more investigations are requested, several recent publications [30,31] showed that electrostatic field would damage the culturability of collected bio-particles (bacteria, fungi and other cellular derivatives) due to the excessively charged stress. Furthermore, the particle collection by unipolar charge systems causes a significant difference compared with real results in monitoring a collection due to the intrinsic charge of bio-particles. It is up to the charge polarities of particles and generator, the error could be up to 50% as represented in [30].

Recently, we have developed a novel method to generate ion winds using two pin electrodes which are placed in parallel with a designed inter-electrode gap [32] . Such configuration allows the ion winds of opposite charge from two electrodes moving forward to the space in front of the electrodes' tips [32–38]. In this work, a new electrostatic aerosol sampling method using bipolar corona dual ion winds is developed. For the present approach, particles collected at a collection chamber are almost neutralized owing to dual ion winds generated by an electric field. Besides, the new configuration also possesses several advantages such as (i) the removal of undesired impediments to airborne particle flow and ion wind along a channel and (ii) the flexibility in choosing various types of material for the sampling chip including non-conductive ones. The performance of the present method is investigated with both experimental work and numerical simulation using OpenFOAM finite volume method.

2. Mechanism of the present aerosol electrostatic sampler

As summarized above, traditional aerosol electrostatic precipitator is configured by one discharge electrode and one counter electrode acting as the sampling electrode for the particle collection [23–25] (see Fig. 1a). Thus, the sampling electrode must be conductive and therefore it is not suitable with several biocompatible materials, such as polydimethylsiloxane, polymethylmethacrylate or silicone gel. Moreover, since the conventional EP creates a considerable amount of charge, it is not appropriate for bio-sampling in several cases as mentioned in section 1. In addition, it proved to be challenging to segregate charged droplets from a plate due to the presence of Van-de-Wall force. This issue has recently attracted to numerous researches on bio-aerosol sampling using a solvent on the lab-on-chip interface termed as the aerosol-to-hydrosol transfer [39–42].

For our research, the new technique to collect airborne particles of zero net charge is developed using a dual ion wind based generator (see Fig. 1b). The mechanism of the scheme is described as follows. With a high voltage applied between two parallel pin electrodes, a curved electric field is generated and expands outward the space between the two electrodes and then induces two ion winds simultaneously as shown in Fig. 1b. The two ion

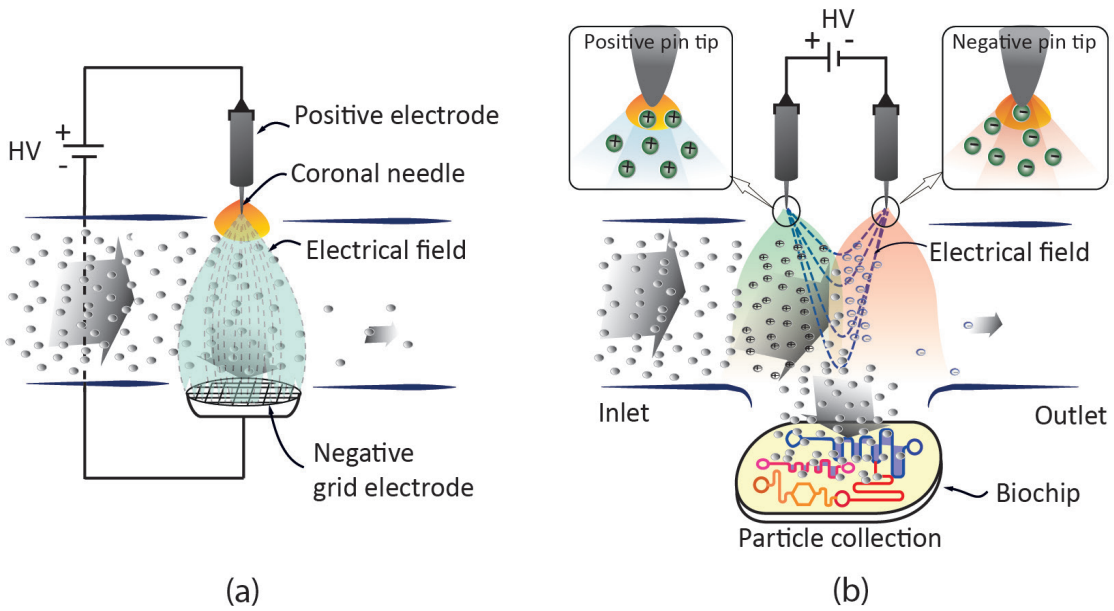

Figure 1. Configuration and mechanism of a bioaerosol electrostatic samplers. (a) Traditional configuration: High voltage is applied between discharged electrode and the collector to generate a high electric field, the collector is a part of high voltage circuit. (b) The present configuration: High voltage is separated from the collector; Electric field between two discharge electrodes creates ion winds. Particles are neutralized and directed towards the collector under the effect of the electric field and ion winds.

winds have the same but opposite charges. Regardless of the initial charge of the entrance particles, they are charged by the electric field while moving through the channel. Under the interaction with the ion wind at the upstream positive electrode, the aerodynamic force by ion wind and the electrostatic force drift charged particles toward a particle sampling chip (collector) installed in the opposite side of the electrodes. On the way to the collector, charged particles move downstream due to its initial airflow momentum and the curved electric field, and continue interacting with the negative ion wind from the downstream electrode. The negative ion wind further pushes particles toward the opposite side of the channel and neutralizes their charge as shown in Fig. 1b. As a result, the net charge of airborne particles is alleviated or even neutralized when they reach the collector due to the charge balance from two ion winds [37].

As presented, since neither the electrodes nor the sampling chip is installed inside the channel, there is not any impediment on the way of the airborne particles and the ion winds. Due to the insulation of sampling chip from the ion winds generating circuit, various materials can be used for the collector including glass, gel, metal or semiconductor. As the airborne particles sampled with very low net charge, the present scheme should be suitable for developing bio-aerosol electrostatic precipitator.

3. Experiment setup

3.1 Sampler prototype

A schema of the present aerosol sampler prototype is shown in Fig. 2. The system consists of a channel made of polypropylene for the aerosol, an ion wind generator assisting the sampling process and a sampling chamber for particle collection. The circular shaped inlet and outlet parts are connected smoothly with a body of 15 x 15 mm^2 rectangular cross-section and 70 mm length to avoid possible abruptions of the aerosol flow. As proposed by Asbach et al., [43] Tygon is selected as a material for two connecting tubes at the upstream and downstream of the channel to minimize the particle loss during the experiment. The ion wind generator is installed in the upper side of the channel centre while the sampling chamber is in the opposite side with an insulated tray of acrylic glass (see Fig. 2).

The ion wind generator consists of two stainless steel SUS304 electrodes placed in parallel with each other, both with 8 mm length and 0.5 mm diameter. The two electrodes with tip size of 80 µm are fixed inside a holder insulated from surroundings. The tips of electrodes are placed in a hole, 2 mm away from the wall in order not to cause an obstacle along the flow of particles as well as to protect the flow from undesired contaminants by electrodes. A battery-operated high voltage generator capable of generating up to 10 kV DC voltage is connected to the electrodes. In order to prepare the experiment, the air velocity is determined using a conventional air flow meter (AWM5102VN) to establish the velocity profile inside the channel. The current and voltage (I-V)

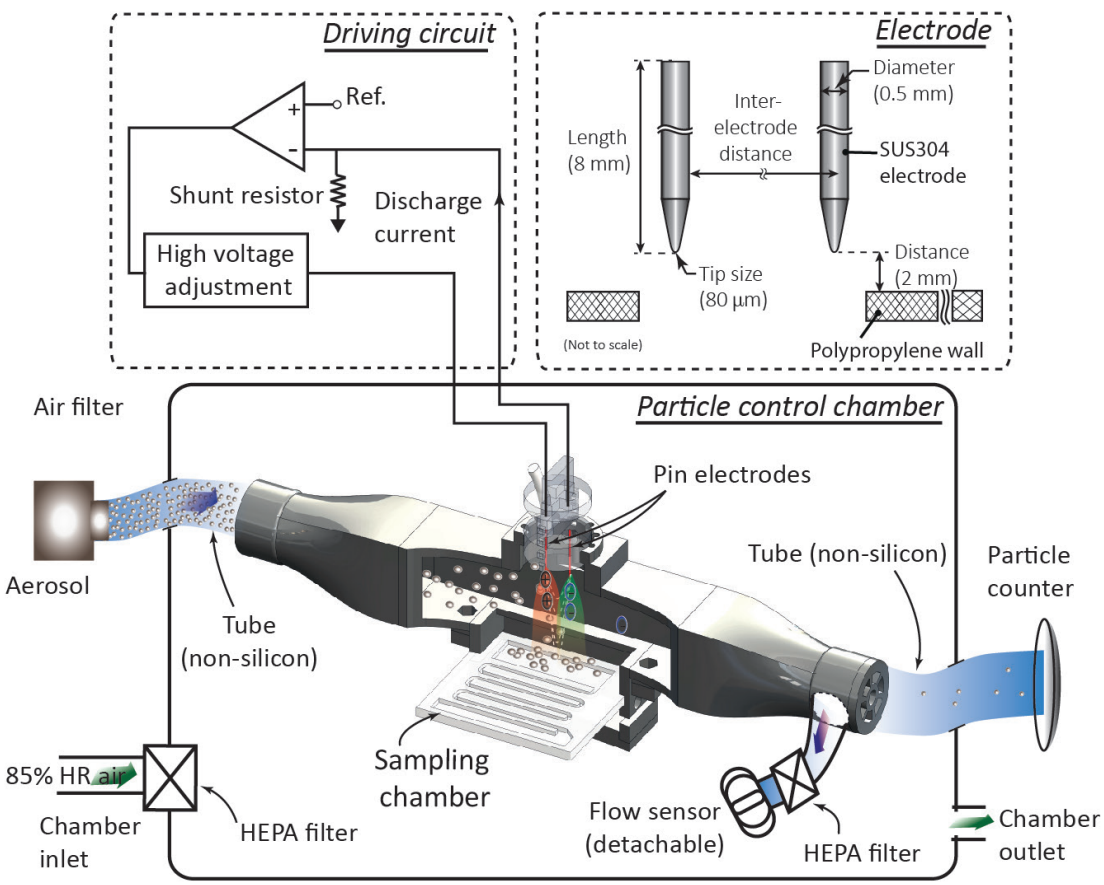

Figure 2. The present aerosol electrostatic sampler (AES): A schema of the AES together with its mechanism and configuration.

characteristic of ion wind is recorded for an entire range of air flow rates throughout the experiment by an oscilloscope (HAMEG-R&S). The experiment was carried out with the ambient temperature of 24 - 25 °C, relative humidity of 55% – 65% and the atmospheric pressure in a control box of the size of 25 cm × 40 cm × 65 cm, where clean air is supplied through a filter (HEPA).

3.2. Measurement protocol

The efficiency of the present particle sampler is investigated based on the ratio of number of particles counted at the outlet of channel in the two cases with and without the effect of ion winds for a given flow rate as follows [24].

$$\eta = 1 - \frac{N_{outlet-On}}{N_{outlet-Off}}, \quad (1)$$

where $N_{outlet-on}$ and $N_{outlet-off}$ are the particle concentrations measured at the air flow channel outlet with and without the corona discharge, respectively.

For experiment, particles collected on the tray are followed up by an optical microscope and counted by a particle counter. A sample of polystyrene particles with diameter of 1.0 µm is diluted with deionized water, filtered by 0.2 µm nano-porosity membrane (Merck Millipore Ltd), and stored in room condition for 30 minutes. The particles are then stirred up by a mild ultrasonic mixer to prevent their agglomeration and then introduced into an aerosol generator placed at the inlet of channel. Although the system can be operated with a large range of particle sizes to simulate a natural human breath, at this step the trace by a sample of only one particle size of 1 µm allows to investigate easily but efficiently the performance of the device.

The influence of corona parameters on the efficiency of the present device can be investigated using the Deutsch-Anderson equation [44] as follows.

$$\eta = 1 - e^{-\frac{n_p e C_C E}{3\pi\mu d_p} \times \frac{A}{Q}}, \quad (2)$$

where A is the collecting area; n_p the particle charge; *e* the elementary charge; C_C the slip correction factor; *E* the electric field; μ the viscosity; *Q* the flow rate of aerosol and d_p the particle diameter. Eq. (2) depicts that collection efficiency increases with the increase of particle charge (n_p) but with the decrease of flow rate.

The measurement protocol proceeds as follows. One minute after turning on the aerosol generator, a high voltage is applied on the two electrodes to induce a corona discharge current. Until the current reaches a stable state, an aerosol meter (TSI 9306) is switched on to start measuring the particle concentration every 20 seconds. This measurement process is repeated five times and the experiment is conducted with a range of flow rates from the generator. The process is controlled by a compressor and monitored at the channel outlet using a flow sensor AWM5102VN (Honeywell, USA). Experimental results are presented in the next section.

3.3. Experimental results and discussions

A range of flow rates of particles (2.0 lpm to 6.5 lpm) is used to investigate the efficiency of the present device with different applied voltages. In this range of flow rate, the initial charge of the aerosol is confirmed by an electrometer (3068 TSI) to be less than -50 fA. The densities of particles measured in the sampling chamber and at the outlet with and without the effect of ion winds are plotted in Fig. 3 where the aerosol includes polymer particles of 1.0 µm.

The results in Fig. 3 show that polymer particles almost move to the collecting tray under the effect of ion winds. Indeed, the concentration of particle flow measured at the outlet without the ion wind is almost identical with the concentration of particles measured in the sampling chamber when turning on the ion wind.

Theoretically, the particle charge increases with the increase of ion wind density and thus with the increase of voltage [44]. In other words, the collection efficiency increases with the increase of voltage applied on the two electrodes. Experimental results presented in Figs. 4 and 5 calculated from Eq. (1) are in good agreement with the statements above and by Eq. (2) on the relationships of the collection efficiency of the present approach to the flow rate of particles and the applied voltage, respectively.

Indeed, Fig. 4 shows that the collection efficiency of the system decreases with the increase of the aerosol flow rate using an applied voltage of 5.5 kV. In addition, after reaching a maximum value of 94%, the efficiency starts decreasing since the flow rate of 4 lpm. Meanwhile, the efficiency increases with the increase of applied voltage with any flow rate of aerosol as shown in Fig. 5. It can be seen that with a relevant discharge voltage, the new configuration is preferable to several ones published [24] whose efficiency is from 40% to 90% compared with from 87% to 94% of the present system.

The research is extended with several samples included different particle sizes with a range of diameters from 300 nm to 1000 nm. For such experiments, aerosols include polymer particles of 1.0 µm and water particles created by water atomizing using an aerosol generator (ATM 226). The distribution of different particle sizes at the sampling chamber when turning on and off ion wind presented in the inset of Fig. 6 depicts that almost particles of different sizes are drifted by the wind generated at a voltage 5.5 kV toward the sampling chamber, meanwhile a small percentage of particles was found at the collector with the absence of ion wind.

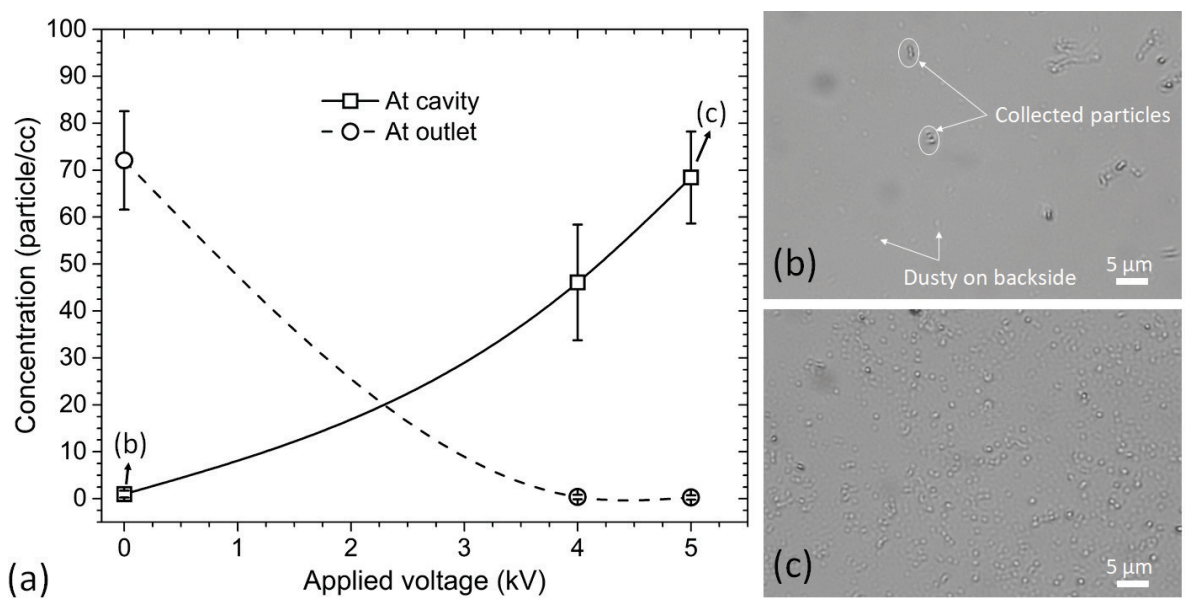

Figure 3. Experimental results of the present aerosol electrostatic sampler: Density of particles collected at the outlet of the channel and the sampling chamber using polymer particles with diameter of 1.0 µm (Fig.3a). Images of collected particles (small cycles) in the sampling chamber without the use of ion wind (Fig. 3b) and with ion wind (Fig. 3c) which are observed using an optical microscopic.

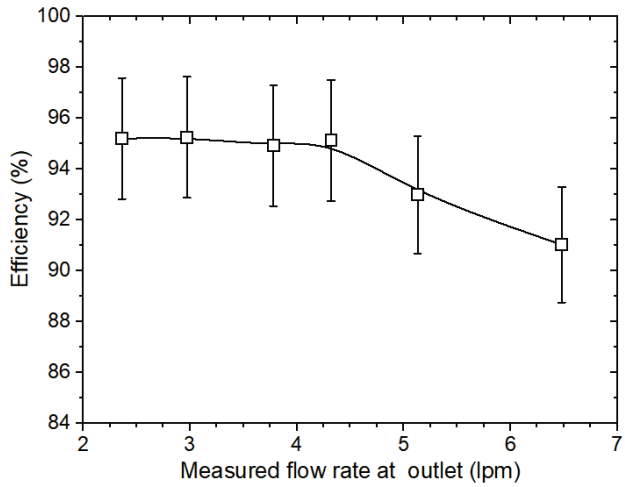

Figure 4. Experimental results of the present aerosol electrostatic sampler: The efficiency of the present device plotted versus the flow rate of particles with polymer diameter of 1.0 µm using an applied voltage of 5.5 kV and inter-electrode distance of 8.0 mm.

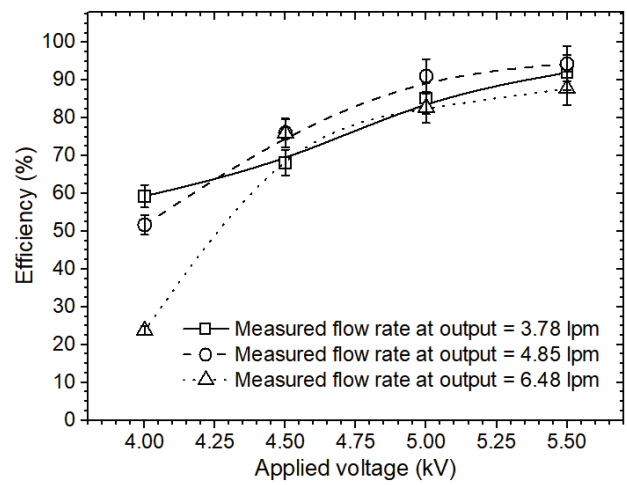

Figure 5. Experimental results of the present aerosol electrostatic sampler: The efficiency of the present device plotted versus the applied voltage for several different flow rates (3.78, 4.85 and 6.48) lpm of particles with diameter of 1.0 µm and using inter-electrode distance of 8.0 mm.

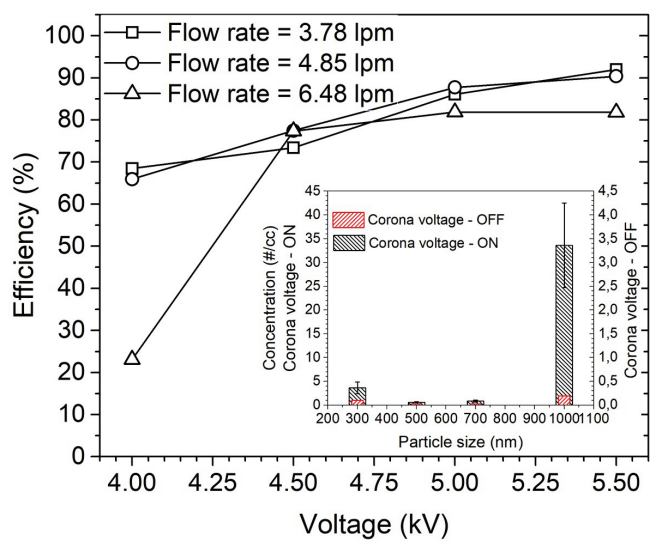

Figure 6. The efficiency of the present device plotted versus the applied voltage with several different flow rates (3.78, 4.85 and 6.48) lpm of aerosol with particles of different diameters using inter-electrode gap of 8.0 mm.

The inset shows a distribution of particles collected in the sampling chamber using aerosol of different particle sizes with and without the ion wind. A flow rate of 3.78 lpm included polymer particles of 1.0 µm (1000 nm) and smaller water particles is used. Inter-electrode distance is 8.0 mm

Similar to the aerosol of particles with one unit size, the collection efficiency determined by Eq. (1) for the whole measured particles, increases with the increase of applied voltage with any flow rate of aerosol as shown in Fig.

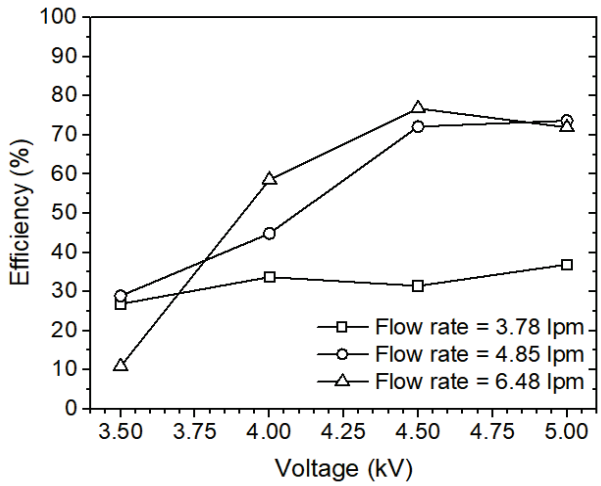

Figure 7a. The efficiency of the present device plotted versus the applied voltage with several different flow rates (3.78, 4.85 and 6.48) lpm of particles of 1.0 µm using the inter-electrode distance of 5mm.

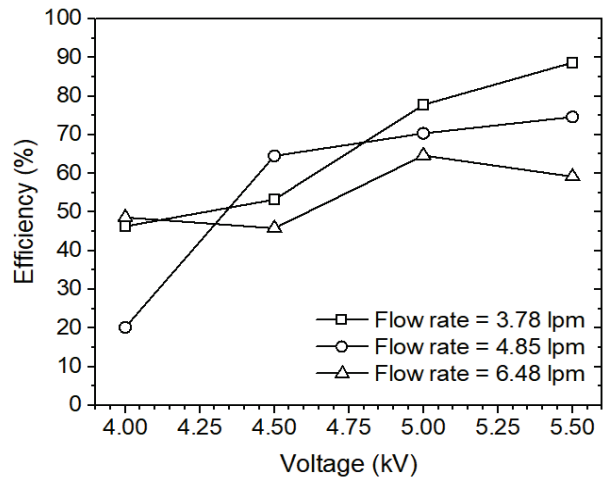

Figure 7b. The efficiency of the present device plotted versus the applied voltage with several different flow rates (3.78, 4.85 and 6.48) lpm of particles of 1.0 µm using the inter-electrode distance of 10 mm.

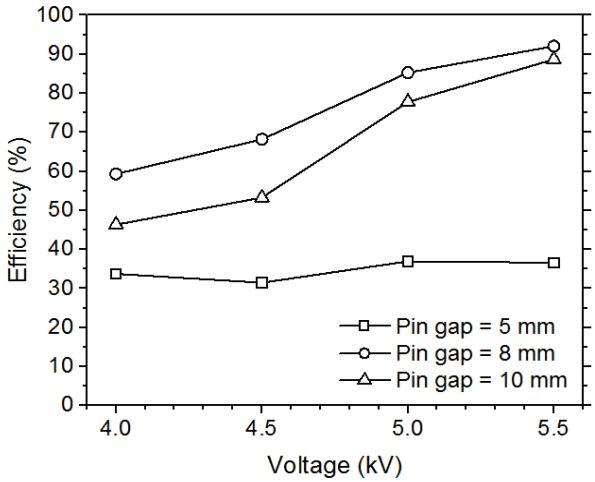

Figure 7c. The efficiency of the present device plotted versus the applied voltage with several different inter-electrode distances (5, 8, 10) mm and a flow rate of 3.78 lpm with particles of 1.0 µm.

6. In addition, the difference of collection efficiency is insignificant for different flow rates after the applied voltage overcame 5.0 kV and the efficiency reaches a maximum value at the applied voltage of around 5.5kV.

Besides applied voltage, the effect of inter-electrode distance on the efficiency of the present device is also considered for aerosol with polymer particles of 1.0 µm. Experimental results by Figs. 7a & b show that the effect of the inter-electrode distance on the efficiency of sampler depends on the flowrate of aerosol. For example, the efficiency is the highest with the inter-electrode distance of 5 mm (Fig. 7a) but the lowest with the distance of 10 mm (Fig. 7b) using the same aerosol flowrate of 6.48 lpm. In other words, there is relevant flowrate for a designed inter-electrode distance of the present device. For example, the flow-rate of 3.78 lpm is relatively relevant for

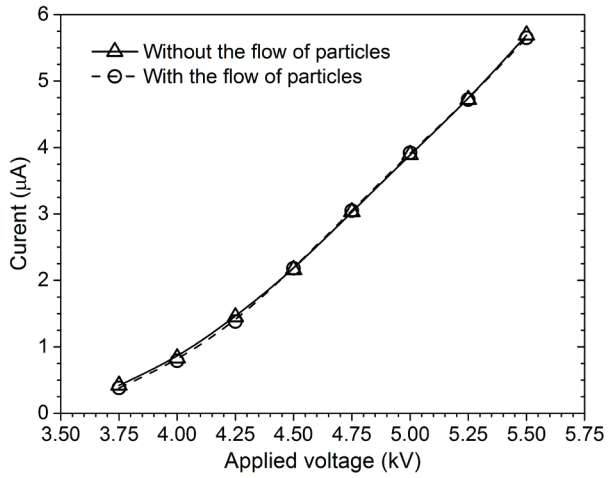

Figure 8. I-V characteristics of corona measured with and without the flow of particles during the discharge process.

the inter-electrode distance of 8 mm compared with the distances 5mm and 10mm because it yields a higher efficiency of the device as given in Fig. 7c.

Furthermore, the charge of the particle flow throughout the channel measured by an electrometer probe (3068 TSI) installed in the device is approximately -10 fA, which is much lower than one of microamperes as presented recently in [37]. In other words, the airborne particles are nearly neutralised by the positive and negative ion winds.

For the present configuration of sampler, powers used for the corona discharge and the device operation are very low, around 20 mW and 70 mW, respectively. This allows the present device to be operated by a small battery, which is promising in the development of portable sampling devices. Finally, the experiment also demonstrates that particles can be deposited on a sampling tray which is made entirely of glass. It means that insulating materials are applicable for collectors in the present system.

4. Numerical simulation of the new configuration

The simulation of particle flow through the device under the effect of ion winds is presented in this section. The numerical results are then compared with experimental ones presented in section 3. A multi physic simulation is carried out to analyze the characteristics of the present configuration, in which several experimental results on corona discharge are introduced as the boundary conditions of the problem. In this work, we consider three issues: (i) the electro-hydrodynamics for the generation of ion winds; (ii) the charging process of particles caused by a strong electric field and (iii) the migration of charged particles drifted by the fluidic and electrostatic forces.

4.1. Governing equations and boundary conditions

For the electro-hydrodynamics, by neglecting the buoyancy force due to temperature variation, ion wind is considered as an incompressible turbulent flow of ions where the ionization region surrounding the electrode tips is modeled with a corresponding charge concentration. At the steady state, the migration of ions in the inter-electrode zone, the interaction of ions within the electric field and the charge consumption by the ion

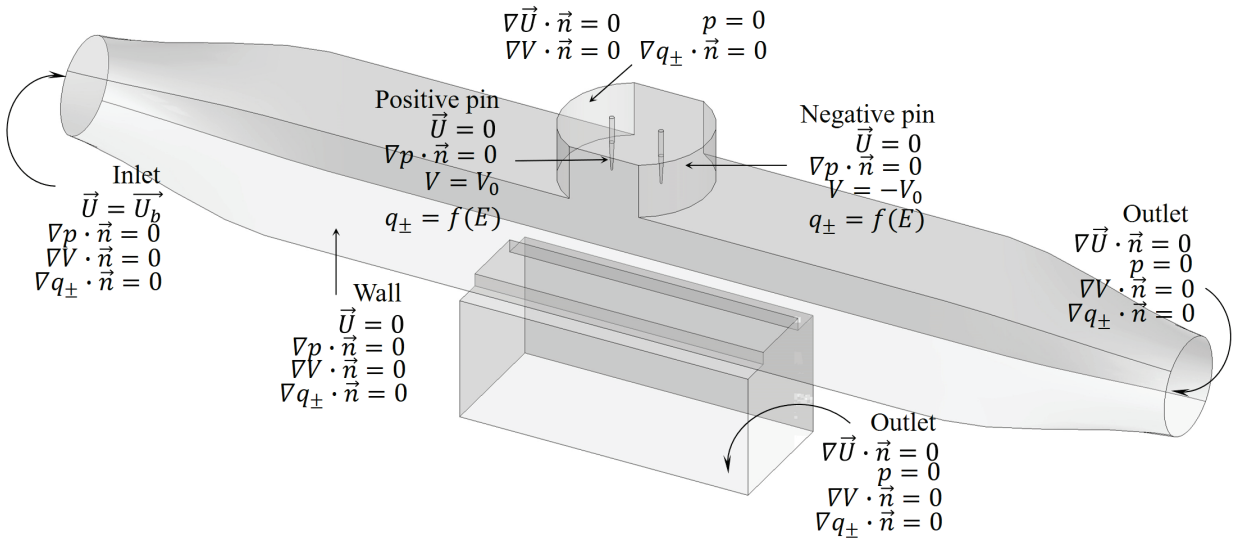

Figure 9. Simulation of the present sampler: considered domain and boundary conditions.

recombination process are governed by the Gauss' law of electrical field and the conservations of charge, momentum and mass as follows [45–47].

$$\vec{E}=\nabla\emptyset, \tag{3a}$$

$$\nabla\cdot\left(\pm\mu\vec{E}\rho_{\pm}\pm\vec{U}\rho_{\pm}\right)=-R_i\rho_+\rho_-/q_e, \tag{3b}$$

$$\nabla\cdot(\nabla\emptyset)=-(\rho_+-\rho_-)/\varepsilon_0, \tag{3c}$$

$$\nabla\cdot\left(\vec{U}\vec{U}\right)-\nabla\cdot\left(\nu\nabla\vec{U}\right)=-\nabla p+f_e/\rho_a, \tag{3d}$$

$$\nabla\cdot\vec{U}=0, \tag{3e}$$

$$f_e=(\rho_+-\rho_-)\vec{E}, \tag{3f}$$

where μ is the mobility of positive and negative charges ($\mu=\ 1.6\times10^{-4}m^2\cdot V^{-1}\cdot s^{-1}$); R_i =$10^{-13}m^3\cdot s^{-1}$ the rate constant for ion-ion recombination; q_e= 1.62×10-19 C the charge of electrons; $\vec{U}$ velocity of air drifted by the motion of charge; $\epsilon_0=\ 8.854\times10^{-12}\ C\cdot V^{-1}\cdot m^{-1}$ the permittivity of the air; p the pressure; $\nu=15.7\times10^{-3}m^2\cdot s^{-1}$ the kinematic viscosity, and $\rho_a=\ 1.2041kg\cdot m^{-3}$ the air density.

The ion density of corona is assumed to be constant ($\rho_{\pm}=I/(\mu E_w a)$) on the face of electrodes, where a is the area of electrode tips, E_w the electric field at electrode tips determined by the Peek's law for air: $E_w=31(kV/cm)[1+0.308/(0.5R)^{1/2}]$, with R being the radius of electrode tips in cm and I the corona discharge current given by the I-V experimental characteristics in Fig. 8. The current in Fig. 8 was measured at the negative electrode for cases with and without air flow and accordingly used as boundary conditions in simulation. Because both electrodes are connected to a single power source, which is battery operated, this current is considered to be equal at both positive and negative electrodes based on the simplified Kirchhoff's current law for charge conservation. In this work, the particle flow does not significantly affect the corona discharge because (i) there is

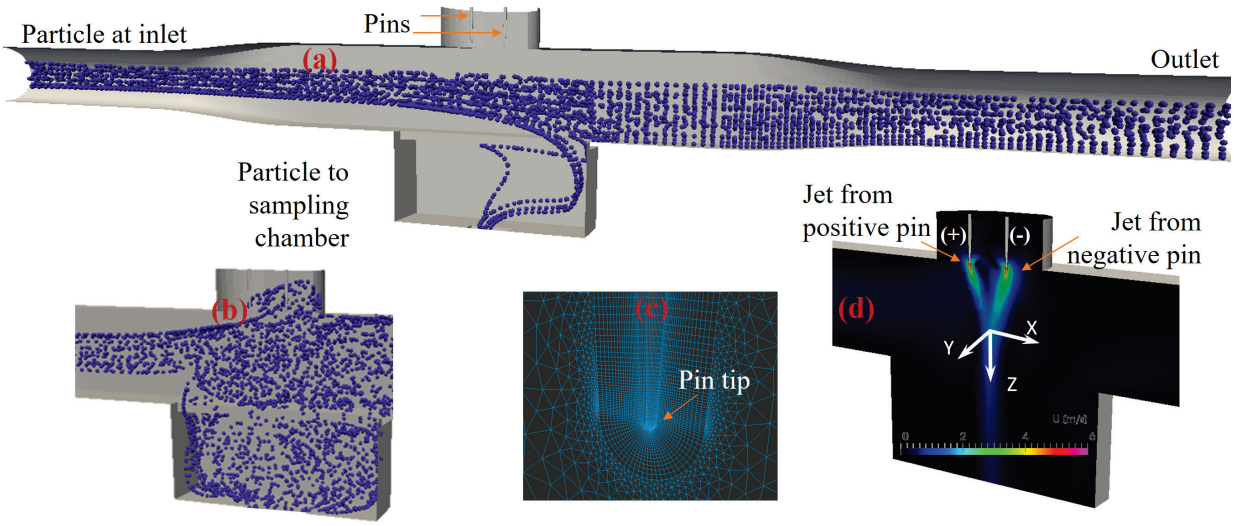

Figure 10. Simulation of the present device: Particle trajectories from the numerical simulation with ion wind is off (a), ion wind is on (b), meshing at the vicinity of pin tips (c) and ion wind from the dual electrodes (d).

no obstacle along the channel as presented in section 3 and (ii) the maximum velocity of particle flow is less than 1 m/s [48–51].

Neglecting the random motion [52], ions drift along the electric field lines to reach and charge particles. The charging rate is determined by the following equation [53,54].

$$\frac{dq}{dt} = \pi\epsilon_0\rho_o\mu q_s\left(1-\frac{q}{q_s}\right)^2, \tag{4}$$

where q_s the saturation charge of particles and given by $q_s = \left(1+2\frac{K-1}{K+2}\right)r_p^2E/\epsilon_0$, with r_p the radius of the particle; K the dielectric constant of particles and ρ_o the ion concentration in the vicinity of particles.

Particles' locations and their velocities are tracked by the Newtonian second law as follows.

$$m_p\frac{d\overrightarrow{U_p}}{dt} = \overrightarrow{f_D} + \overrightarrow{f_E}, \tag{5}$$

where m_p is the mass of a particle, f_D the drag force of air acting on the particle. f_E is the Coulomb's force of the electric field since the particle is charged with q_p and given by

$$\overrightarrow{f_E} = q_p\overrightarrow{E_p}\,, \tag{6}$$

with $\overrightarrow{E_p}$ the electric field projected onto the particle position, meanwhile the drag force f_D is determined by

$$\overrightarrow{f_D} = \frac{1}{2}C_D\rho_a A\left(\vec{U}-\overrightarrow{U_p}\right)\left|\vec{U}-\overrightarrow{U_p}\right|, \tag{7}$$

where C_D is the drag coefficient, ρ_a the air density, $\vec{U}-\overrightarrow{U_p}$ the difference between the air and particle velocities at a position of the particle. In this simulation, particles are assumed to be sphere whose surface area is $A = \pi d^2$ with d the diameter of particle.

The drag coefficient (C_D) is then computed by the Shiller-Neumann correlation [55]

$$C_D = \frac{24}{Re_p}\left(1 + 0.15{Re_p}^{0.687}\right), \quad (8)$$

where Re_p is the Reynolds number $Re_p = \rho_a D \left|\vec{U} - \overrightarrow{U_p}\right| / \mu_g$ with ρ_a the viscosity of air.

At an instant, with an obtained velocity of particles, their position $\overrightarrow{x_p}$ is determined straightforwardly by the following kinematic equation

$$\frac{d\overrightarrow{x_p}}{dt} = \overrightarrow{U_p} \quad (9)$$

Figure 9 represents the domain under consideration together with boundary conditions of the problem. A set of 400 particles with diameter of 1.0 µm is introduced into the system. The charge of particles is calculated at the saturated state q_s. The velocity profile of particle flow, electric field lines, generated ion wind and particles' trajectory are determined using OpenFOAM finite volume based solver [56,57].

4.2. Numerical results and discussion

With a meshing at the vicinity of electrode tips as described in Fig. 10c, the ion wind generated at the electrodes is given in Fig. 10d. In addition, trajectories of particles in the device without and with the use of ion wind by 5.5 kV are represented in Figs. 10a&b, respectively. The numerical results show that there is approximately 62% of particles reaching the sampling chamber with ion wind generated by a voltage of 5.5 kV compared with 13% without ion wind.

The simulation is repeated with a range of applied voltages V = (4.0 - 5.5) kV using a flowrate of 5.0 lpm. Numerical experiments show that the number of particles reaching the sampling chamber and thus, the efficiency of the sampler increases with the increase of applied voltage as shown in Fig. 11. These simulated results are in agreement with ones by the experiments using the same parameters except a small difference of the flowrate of particle flow (4.86 lpm vs. 5.0 lpm) as presented in Fig. 5.

The linear relation between the efficiency and applied voltage with the flowrate of 5lpm observed by both experimental and simulation works (Figs. 5 and 11) allows to predict the characteristics of the present aerosol sampler. In addition, the percentage of lost particles by the present approach is significantly improved, it is 18% compared with 26% by a point-to-plane system reported in [58]. Nevertheless, the particle loss depends on the design of an aerosol sampling system and hence, it is necessary to further consider for specific applications which are the object of our ongoing work.

Finally, the simulation is also extended with aerosol of particles with different sizes ranging 200 to 2000 nanometres using a flowrate of 3.78 lpm, applied voltage of 4.5 kV and inter-electrode distance of 8.0 mm. At the inlet, 400 particles are introduced into the system through a circular area whose diameter is 0.75 of that of the inlet. The particles' size satisfies the Gauss distribution with the mean diameter of 1µm and a standard deviation 3σ covering the range 200 nm – 2000nm. Since particles with different quantities are randomly released, while moving inside the channel, random correlations of particle sizes and initial positions are determined. Thus, the number of particles of a size is possibly lost more than others, and this yields a variation of the collection efficiency for particles with different sizes. Fig. 12 represents the particle distribution in the device, especially at the collecting chamber with and without the use of ion winds. The simulation results show that the efficiency of the collection vibrates from 50% to 73% for the particle sizes smaller than 1µm. The efficiency then gradually decreases with particle size bigger than 1µm. This can be explained as the inertia effect on the electrostatic force

for particles having a significant mass. In addition, the numerical results by Fig. 12c show an agreement with the experimental one in Fig. 6 where the effect of ion wind was observed for a range of particle sizes

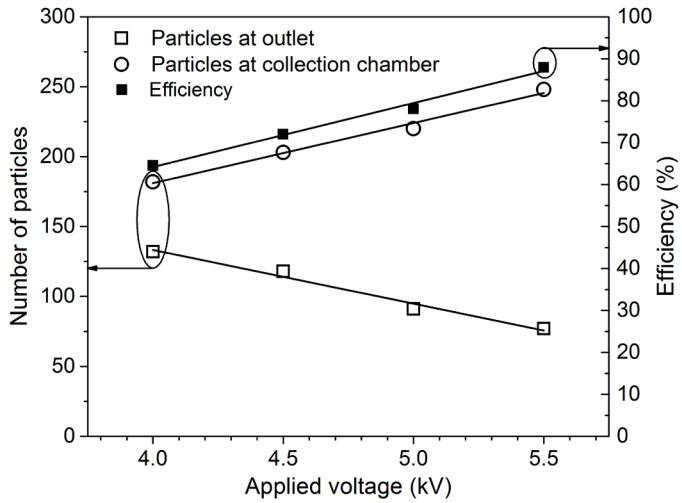

Figure 11. Simulation of the sampler: Efficiency of the present sampler at different applied voltages with the flow rate of 5 lpm and the number of particles released at inlet = 400

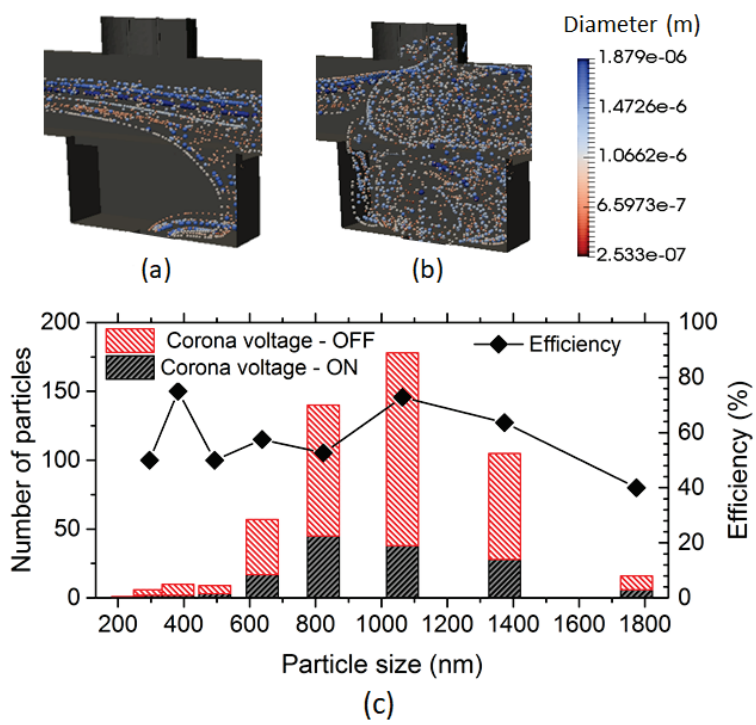

Figure 12. Numerical simulation of the present device using aerosol of different particle sizes: Particle trajectories in the sampling chamber by the simulation without ion wind (a) and with ion wind (b); Particle distribution and efficiency using ion wind generated by an applied voltage of 4.5kV (c).

Although the numerical simulation reasonably reflected the characteristics and behaviours of the device compared with experimental results, it is necessary to consider and investigate several problems in our future work, including the difference between negative and positive ions; the introduction of the diffusive charging of particles which dominates the charging system for nano-particles; the coalescence and effect of shape for submicron particles (less than 0.1μm) [59,60]; and the role of charging by electrostatic force, drifting by aerodynamic force and the electro-coalescence in a simulation model [61,62] .

5. Conclusion

A new electrostatic sampling method based on dual ion winds has been developed to collect particles without net charge. For the approach, a flow of airborne particles moves through a channel under the effect of dual ion winds of opposing charges generated simultaneously by electrodes arranged in parallel. As results of the new configuration, airborne particles can move smoothly through the device to reach the collection chamber because there is not any impediment along the channel. In addition, particles reaching to sampler are almost neutralized due to corona dual ion winds. Another advantage of the present approach is that the material of sampling chip can be chosen arbitrarily including glass, gel, metal or semiconductor owing to the isolation of sampling chip from ion winds generating circuit. The present aerosol sampling method is investigated by experimental work for a range of discharge voltages (4.0 kV to 5.5 kV) and flow rates of airborne particles (2.0 to 6.5 lpm). A numerical simulation is also carried out and numerical results support those by experiments. Although further investigation is required, the present approach would yield a promising platform for a system of automated bio-aerosol sampling.

Reference

[1] L. Morawska, A. Afshari, G.N. Bae, G. Buonanno, C.Y.H. Chao, O. Hanninen, et al., Indoor aerosols: From personal exposure to risk assessment, Indoor Air. 23 (2013) 462–487. doi:10.1111/ina.12044.

[2] Y. Song, X. Li, X. Du, Exposure to nanoparticles is related to pleural effusion, pulmonary fibrosis and granuloma, Eur. Respir. J. 34 (2009) 559–567. doi:10.1183/09031936.00178308.

[3] X.R. Wang, Y.L. Chiu, H. Qiu, J.S.K. Au, I.T.S. Yu, The roles of smoking and cooking emissions in lung cancer risk among Chinese women in Hong Kong, Ann. Oncol. 20 (2009) 746–751. doi:10.1093/annonc/mdn699.

[4] G.N. Sze-to, C.L. Wu, C.Y.H. Chao, M.P. Wan, T.C. Chan, Exposure and cancer risk toward cooking-generated ultrafine and coarse particles in Hong Kong homes, HVAC&R Res. 18 (2012) 204–216. doi:10.1080/10789669.2011.598443.

[5] T. Reponen, K. Willeke, S. Grinshpun, A. Nevalainen, Biological Particle Sampling, in: Aerosol Meas., John Wiley & Sons, Inc., Hoboken, NJ, USA, 2011: pp. 549–570. doi:10.1002/9781118001684.ch24.

[6] T. Han, G. Mainelis, Investigation of inherent and latent internal losses in liquid-based bioaerosol samplers, J. Aerosol Sci. 45 (2012) 58–68. doi:10.1016/j.jaerosci.2011.11.001.

[7] X. Lin, K. Willeke, V. Ulevicius, S.A. Grinshpun, Effect of sampling time on the collection efficiency of all-glass impingers, Am. Ind. Hyg. Assoc. J. 58 (1997) 480–488. doi:10.1080/15428119791012577.

[8] S.A. Grinshpun, K. Willeke, V. Ulevicius, A. Juozaitis, S. Terzieva, J. Donnelly, et al., Effect of impaction, bounce and reaerosolization on the collection efficiency of impingers, Aerosol Sci. Technol. 26 (1997) 326–342. doi:10.1080/02786829708965434.

[9] V. Langer, G. Hartmann, R. Niessner, M. Seidel, Rapid quantification of bioaerosols containing L. pneumophila by Coriolis® μ air sampler and chemiluminescence antibody microarrays, J. Aerosol Sci. 48 (2012) 46–55. doi:10.1016/j.jaerosci.2012.02.001.

[10] D. Saini, G.W. Hopkins, C. Chen, S.A. Seay, E.M. Click, S. Lee, et al., Sampling port for real-time analysis of bioaerosol in whole body exposure system for animal aerosol model development, J. Pharmacol. Toxicol. Methods. 63 (2011) 143–149. doi:10.1016/j.vascn.2010.09.002.

[11] B. Ghosh, H. Lal, A. Srivastava, Review of bioaerosols in indoor environment with special reference to sampling, analysis and control mechanisms, Environ. Int. 85 (2015) 254–272. doi:10.1016/j.envint.2015.09.018.

[12] J. Mandal, H. Brandl, Bioaerosols in Indoor Environment - A Review with Special Reference to Residential and Occupational Locations, Open Environ. Biol. Monit. J. 41 (2011) 83–96. doi:http://dx.doi.org/10.2174/1875040001104010083.

[13] Y. Gilbert, C. Duchaine, Bioaerosols in industrial environments: a review, Can. J. Civ. Eng. 36 (2009) 1873–1886. doi:10.1139/L09-117.

[14] A.K. Maddineni, D. Das, R.M. Damodaran, Air-borne particle capture by fibrous filter media under collision effect: A CFD-based approach, Sep. Purif. Technol. 193 (2018) 1–10. doi:10.1016/j.seppur.2017.10.065.

[15] W. Eduard, D. Heederik, Methods for quantitative assessment of airborne levels of noninfectious microorganisms in highly contaminated work environments., Am. Ind. Hyg. Assoc. J. 59 (1998) 113–127. doi:10.1080/15428119891010370.
[16] Z. Li, Y. Liu, Y. Xing, T.-M.-P. Tran, T.-C. Le, C.-J. Tsai, Novel Wire-on-Plate Electrostatic Precipitator (WOP-EP) for Controlling Fine Particle and Nanoparticle Pollution, Environ. Sci. Technol. 49 (2015) 8683–8690. doi:10.1021/acs.est.5b01844.
[17] T.-M.M. Chen, C.-J.J. Tsai, S.Y. Yan, S.N. Li, An efficient wet electrostatic precipitator for removing nanoparticles, submicron and micron-sized particles, Sep. Purif. Technol. 136 (2014) 27–35. doi:10.1016/j.seppur.2014.08.032.
[18] X. Xu, C. Zheng, P. Yan, W. Zhu, Y. Wang, X. Gao, et al., Effect of electrode configuration on particle collection in a high-temperature electrostatic precipitator, Sep. Purif. Technol. 166 (2016) 157–163. doi:10.1016/j.seppur.2016.04.039.
[19] P. Yan, C. Zheng, G. Xiao, X. Xu, X. Gao, Z. Luo, et al., Characteristics of negative DC corona discharge in a wire–plate configuration at high temperatures, Sep. Purif. Technol. 139 (2015) 5–13. doi:10.1016/j.seppur.2014.10.026.
[20] G. Mainelis, Collection of Airborne Microorganisms by Electrostatic Precipitation, Aerosol Sci. Technol. 30 (1999) 127–144. doi:10.1080/027868299304732.
[21] G. Mainelis, A. Adhikari, K. Willeke, S.A. Lee, T. Reponen, S.A. Grinshpun, Collection of airborne microorganisms by a new electrostatic precipitator, J. Aerosol Sci. 33 (2002) 1417–1432. doi:10.1016/S0021-8502(02)00091-5.
[22] G. Mainelis, K. Willeke, P. Baron, S. a. Grinshpun, T. Reponen, Induction Charging and Electrostatic Classification of Micrometer-Size Particles for Investigating the Electrobiological Properties of Airborne Microorganisms, Aerosol Sci. Technol. 36 (2002) 479–491. doi:10.1080/027868202753571304.
[23] A. Miller, G. Frey, G. King, C. Sunderman, A Handheld Electrostatic Precipitator for Sampling Airborne Particles and Nanoparticles, Aerosol Sci. Technol. 44 (2010) 417–427. doi:10.1080/02786821003692063.
[24] M. Tan, F. Shen, M. Yao, T. Zhu, Development of an Automated Electrostatic Sampler (AES) for Bioaerosol Detection, Aerosol Sci. Technol. 45 (2011) 1154–1160. doi:10.1080/02786826.2011.582193.
[25] E.H. Lee, B. Chua, A. Son, Detection of airborne bacteria with disposable bio-precipitator and NanoGene assay, Biosens. Bioelectron. 83 (2016) 205–212. doi:10.1016/j.bios.2016.04.051.
[26] J.-W. Park, H.R. Kim, J. Hwang, Continuous and real-time bioaerosol monitoring by combined aerosol-to-hydrosol sampling and ATP bioluminescence assay, Anal. Chim. Acta. 941 (2016) 101–107. doi:10.1016/j.aca.2016.08.039.
[27] J.-M. Roux, O. Kaspari, R. Heinrich, N. Hanschmann, R. Grunow, Investigation of a New Electrostatic Sampler for Concentrating Biological and Non-Biological Aerosol Particles, Aerosol Sci. Technol. 47 (2013) 463–471. doi:10.1080/02786826.2013.763896.
[28] J.W. Park, C.W. Park, S.H. Lee, J. Hwang, Fast monitoring of indoor bioaerosol concentrations with ATP bioluminescence assay using an electrostatic rod-type sampler, PLoS One. 10 (2015) 1–13. doi:10.1371/journal.pone.0125251.
[29] T.G. Foat, W.J. Sellors, M.D. Walker, P.A. Rachwal, J.W. Jones, D.D. Despeyroux, et al., A prototype personal aerosol sampler based on electrostatic precipitation and electrowetting-on-dielectric actuation of droplets, J. Aerosol Sci. 95 (2016) 43–53. doi:10.1016/j.jaerosci.2016.01.007.
[30] F. Shen, W. Kai, M. Yao, Negatively and positively charged bacterial aerosol concentration and diversity in natural environments, Chinese Sci. Bull. 58 (2013) 3169–3176. doi:10.1007/s11434-013-5852-9.
[31] K. Wei, Z. Zou, M. Yao, Charge levels and Gram (+/-) fractions of environmental bacterial aerosols, J. Aerosol Sci. 74 (2014) 52–62. doi:10.1016/j.jaerosci.2014.04.002.
[32] V.T. Dau, T.X. Dinh, T. Terebessy, T.T. Bui, Ion Wind Generator Utilizing Bipolar Discharge in Parallel Pin Geometry, IEEE Trans. Plasma Sci. 44 (2016) 2979–2987. doi:10.1109/TPS.2016.2580574.
[33] V.T. Dau, T.X. Dinh, T.T. Bui, Jet flow generation in a circulatory miniaturized system, Sensors Actuators B Chem. 223 (2015) 820–826. doi:10.1016/j.snb.2015.09.151.
[34] V.T. Dau, T.X. Dinh, T.T. Bui, C.D. Tran, H.T. Phan, T. Terebessy, Corona based air-flow using parallel discharge electrodes, Exp. Therm. Fluid Sci. 79 (2016) 52–56. doi:10.1016/j.expthermflusci.2016.06.023.
[35] V.T. Dau, T.X. Dinh, T.T. Bui, T. Terebessy, Bipolar corona assisted jet flow for fluidic application, Flow Meas. Instrum. 50 (2016) 252–260. doi:10.1016/j.flowmeasinst.2016.07.005.
[36] V.T. Dau, T.T. Bui, T.X. Dinh, T. Terebessy, Pressure sensor based on bipolar discharge corona configuration, Sensors Actuators A Phys. 237 (2016) 81–90. doi:10.1016/j.sna.2015.11.024.
[37] V.T. Dau, T.X. Dinh, T. Terebessy, T.T. Bui, Bipolar corona discharge based air flow generation with low net charge, Sensors Actuators A Phys. 244 (2016) 146–155. doi:10.1016/j.sna.2016.03.028.
[38] T.X. Dinh, D.B. Lam, C.-D. Tran, T.T. Bui, P.H. Pham, V.T. Dau, Jet flow in a circulatory miniaturized system using ion wind, Mechatronics. 47 (2017) 126–133. doi:10.1016/j.mechatronics.2017.09.007.
[39] B. Traipattanakul, C.Y. Tso, C.Y.H. Chao, Study of jumping water droplets on superhydrophobic surfaces with electric fields, Int. J. Heat Mass Transf. 115 (2017) 672–681. doi:10.1016/j.ijheatmasstransfer.2017.07.096.
[40] T. Han, Y. Nazarenko, P.J. Lioy, G. Mainelis, Collection efficiencies of an electrostatic sampler with superhydrophobic surface for fungal bioaerosols, Indoor Air. 21 (2011) 110–120. doi:10.1111/j.1600-0668.2010.00685.x.
[41] H.N. Phan, A.R. McFarland, Aerosol-to-Hydrosol Transfer Stages for Use in Bioaerosol Sampling, Aerosol Sci. Technol. 38 (2004) 300–310. doi:10.1080/02786820490426183.
[42] M. Wubulihairen, S.Y. Jiang, Z. Ning, Prototype Development and Laboratory Evaluation of an Aerosol to Hydrosol Sampler, Aerosol Air Qual. Res. 15 (2015) 776–785. doi:10.4209/aaqr.2014.08.0175.

[43] C. Asbach, H. Kaminski, Y. Lamboy, U. Schneiderwind, M. Fierz, A.M. Todea, Silicone sampling tubes can cause drastic artifacts in measurements with aerosol instrumentation based on unipolar diffusion charging, Aerosol Sci. Technol. 50 (2016) 1375–1384. doi:10.1080/02786826.2016.1241858.

[44] H. Williams C, Aerosol Technology: Properties, Behavior, and Measurement of Airborne Particles, second, Wiley-Interscience, 1999.

[45] J.S. Townsend, Electricity in Gases, Oxford University Press, 1915. doi:10.1038/095611a0.

[46] J.J. Thomson, G.P. Thomson, Conduction of Electricity Through Gases, London CUP, 1933.

[47] K. Adamiak, Numerical models in simulating wire-plate electrostatic precipitators: A review, J. Electrostat. 71 (2013) 673–680. doi:10.1016/j.elstat.2013.03.001.

[48] M.D. Yamanaka, H. Hirosawa, Y. Matsuzaka, H. Tanaka, “Glow-discharge” ionic anemometer, Rev. Sci. Instrum. 56 (1985) 617–622. doi:10.1063/1.1138245.

[49] C. Marshall, E. Matlis, T. Corke, S. Gogineni, AC plasma anemometer—characteristics and design, Meas. Sci. Technol. 26 (2015) 85902. doi:10.1088/0957-0233/26/8/085902.

[50] N.T. Van, T.T. Bui, T.X. Dinh, T. Terebessy, T.C. Duc, V.T. Dau, A symmetrically arranged electrodes for corona discharge anemometry, in: 2017 19th Int. Conf. Solid-State Sensors, Actuators Microsystems, IEEE, 2017: pp. 1112–1115. doi:10.1109/TRANSDUCERS.2017.7994247.

[51] V.T. Dau, T.X. Dinh, T.T. Bui, T. Terebessy, Corona anemometry using dual pin probe, Sensors Actuators A Phys. 257 (2017) 185–193. doi:10.1016/j.sna.2017.02.025.

[52] S. Chen, C. Lei, J.C. Patterson, Transport of pollutant particles in a reservoir due to diurnal temperature variation, Int. Commun. Heat Mass Transf. 53 (2014) 124–132. doi:10.1016/j.icheatmasstransfer.2014.02.012.

[53] H.J. White, Particle Charging in Electrostatic Precipitation, Trans. Am. Inst. Electr. Eng. 70 (1951) 1186–1191. doi:10.1109/T-AIEE.1951.5060545.

[54] B.Y.H. Liu, H.C. Yeh, On the theory of charging of aerosol particles in an electric field, J. Appl. Phys. 39 (1968) 1396–1402. doi:10.1063/1.1656368.

[55] R. (Roland) Clift, J.R. Grace, M.E. Weber, Bubbles, drops, and particles, Academic Press, 1978.

[56] OpenFOAM®, OpenFOAM® | The OpenFOAM Foundation, (2016). http://openfoam.org/.

[57] Y. Deng, D. Sun, Y. Liang, B. Yu, P. Wang, Implementation of the IDEAL algorithm for complex steady-state incompressible fluid flow problems in OpenFOAM, Int. Commun. Heat Mass Transf. 88 (2017) 63–73. doi:10.1016/j.icheatmasstransfer.2017.08.004.

[58] G. Pardon, L. Ladhani, N. Sandström, M. Ettori, G. Lobov, Aerosol sampling using an electrostatic precipitator integrated with a microfluidic interface, Sensors Actuators B. Chem. 212 (2015) 344–352. doi:10.1016/j.snb.2015.02.008.

[59] A. Jaworek, A. Krupa, A.T. Sobczyk, A. Marchewicz, M. Szudyga, T. Antes, et al., Submicron particles removal by charged sprays. Fundamentals, J. Electrostat. 71 (2013) 345–350. doi:10.1016/j.elstat.2012.11.028.

[60] M. Mohammadi, Numerical and experimental study on electric field driven coalescence of binary falling droplets in oil, Sep. Purif. Technol. 176 (2017) 262–276. doi:10.1016/j.seppur.2016.12.015.

[61] B.B. Wang, X.D. Wang, T.H. Wang, G. Lu, W.M. Yan, Electro-coalescence of two charged droplets under constant and pulsed DC electric fields, Int. J. Heat Mass Transf. 98 (2016) 10–16. doi:10.1016/j.ijheatmasstransfer.2016.02.083.

[62] L. Liu, W. Wei, H. Yu, J. Zhu, T. Laminger, W. Höflinger, Experimental study on particle removal with gas-liquid cross-flow array system, Sep. Purif. Technol. 174 (2017) 194–202. doi:10.1016/j.seppur.2016.10.021.